Relative importance and interactions of primary and secondary ice production in the Arctic mixed-phase clouds

Xi Zhao[1] and Xiaohong Liu[1]

[1]Department of Atmospheric Sciences, Texas A&M University, College Station, Texas 77840, USA

Correspondence to: Xiaohong Liu (xiaohong.liu@tamu.edu)

Abstract

A discrepancy of up to 5 orders of magnitude between ice crystal and ice nucleating particle (INP) number concentrations was found in the measurements, indicating the potential important role of secondary ice production (SIP) in the clouds. However, the relative importance and interactions between primary and SIP processes remain unexplored. In this study, we implement five different ice nucleation schemes as well as physical representations of SIP processes (i.e., droplet shattering during rain freezing, ice-ice collisional break-up, and rime splintering) in the Community Earth System Model version 2 (CESM2). We run CESM2 in the single column mode for model comparisons with the DOE Atmospheric Radiation Measurement (ARM) Mixed-Phase Arctic Cloud Experiment (M-PACE) observations. We find that the model experiments with aerosol-aware ice nucleation schemes and SIP processes yield the best simulation results for the M-PACE single-layer mixed-phase clouds. We further investigate the relative importance of ice nucleation and SIP to ice number and cloud phase as well as interactions between

22   ice nucleation and SIP in the M-PACE single-layer mixed-phase clouds. Our results show

23   that SIP contributes 80% to the total ice formation and transforms ~30% of pure liquid-

24   phase clouds simulated in the model experiments without considering SIP into mixed-

25   phase clouds. We find that SIP is not only a result of ice crystals produced from ice

26   nucleation, but also competes with the ice nucleation. Conversely, strong ice nucleation

27   also suppresses SIP by glaciating mixed-phase clouds.

1 Introduction

29   Ice crystals significantly impact microphysical and radiative properties of mixed-

30   phase clouds (Korolev and Isaac 2003; Korolev et al., 2017; Morrison et al., 2012), which

31   further impact the Earth's energy budgets. Ice particles in mixed-phase clouds with

32   temperatures between about -38 ℃ and 0 ℃ can be formed via heterogeneous ice

33   nucleation on ice nucleating particles (INPs) or arisen through secondary ice production

34   (SIP) (Kanji et al., 2017; Field et al., 2017). There are three identified heterogeneous ice

35   nucleation mechanisms, namely, contact, deposition, and immersion/condensation

36   freezing. Dust is generally considered as the most effective INPs for heterogeneous ice

37   nucleation at temperatures below about -15 ℃ (Hoose et al., 2008; Atkinson et al., 2013;

38   Kanji et al., 2017). SIP processes generate additional ice crystals, often involving the

39   primary ice. Several SIP mechanisms have been suggested: rime splintering (also known

40   as the Hallett–Mossop (HM) process), droplet shattering during rain freezing (FR), ice-

41   ice collisional break-up (IIC), and fragmentation during the sublimation of ice bridge

42   (Field et al., 2017; Korolev et al., 2020). In addition, other microphysical processes such

43   as rain formation and ice growth are important for mixed-phase cloud properties.

44   Regarding ice-related microphysical processes in mixed-phase clouds, some processes,

45   including riming, accretion, and the Wegener–Bergeron–Findeisen (WBF) process can

46   increase the ice mass mixing ratios while have no effect on ice crystal number

47   concentrations (ICNCs). On the other hand, some processes such as ice aggregational

48   growth decrease the ICNCs while have no impacts on the ice mass mixing ratios.

49   A systematically measured discrepancy by up to 5 orders of magnitude between the

50   ICNCs and INP number concentrations has been reported in previous studies (Mossop,

51   1985; Lasher-Trapp et al., 2016; Field et al., 2017), indicating the existence of additional

52   ice production mechanisms in addition to the primary ice production (PIP) or ice

53   nucleation. Moreover, a strong increase in ICNCs over INP number concentrations may

54   suggest that the PIP would be less important once the SIP processes take place in the

55   clouds. However, the relative importance between PIP and SIP to the ice formation in

56   mixed-phase clouds is largely unknown and warrants a further investigation.

57   Previous studies have identified the potential role of PIP in initiating the SIP based

58   on measurements and idealized parcel model simulations. Sullivan et al. (2018) found

59   that clouds with INP concentrations from 0.002 to 0.15 L^{-1} can initiate the IIC

60   fragmentation to produce enough ice crystals based on parcel model simulations. They

61   also indicated that higher INP concentrations enhance the IIC and HM process rates,

62   while the FR rate is not dependent on the INP concentration. Huang et al. (2017)

63   suggested that a number concentration as low as 0.01 L^{-1} for primary ice is sufficient to

64   generate secondary ice though the HM process in the cumulus clouds observed over the

65   British Isles during the Ice and Precipitation Initiation in Cumulus (ICEPIC) campaign.

66   Crawford et al. (2012) found that a small amount of primary ice (0.01 L^{-1}) could produce

67   enough ice crystals with concentrations up to 100 L^{-1} through the SIP processes in a

68   shallow convective cloud over the UK. Beard (1992) found that the droplet shattering can

69   be initiated by primary ice with a number concentration of ~0.001 L^{-1} in the

70   measurement of a warm-base convective cloud. Albeit these studies, how the SIP

71   processes depend on the PIP and whether PIP promotes the SIP are not explored in the

72   Arctic mixed-phase stratus clouds.

73   SIP is not only a result of PIP, but also can interact with and may even suppress the

74   subsequent PIP. A previous study indicated a 40% decrease of heterogeneous ice

75   nucleation after implementing the SIP into a model (Phillips et al., 2017b), because some

76   of the mixed-phase clouds with weak ascents and low humidities are fully glaciated and

77   become ice-only phase. The influence of SIP processes on PIP is far less investigated

78   compared to the limited studies of PIP influence on the SIP.

79   The goal of this study is to investigate the relative importance of PIP and SIP to

80   ICNCs and their interactions in the Arctic mixed-phase stratus clouds. We are attempting

81   to address the following scientific questions: Is the PIP still important for ICNCs once the

82   SIP processes take place? What effect does the PIP have on the SIP processes? Once

83   happening, how do the SIP processes affect the following PIP through the cloud

84   microphysical processes? This paper is organized as follows. Section 2 introduces the

85   model and the model parameterizations we used in this study. Section 3 describes the

86   model setup and model experiments. Section 4 presents the model results and comparison

87   with observations. The main findings of this study are summarized in section 5.

88

89 2 Model and Parameterizations

90 2.1 Model description

91   This study uses the Community Atmosphere Model version 6 (CAM6), the

92   atmosphere component of the Community Earth System Model version 2 (CESM2)

93   (Danabasoglu et al., 2020) for all the model experiments. In CAM6, the cloud

94   microphysics is represented by a double-moment scheme (Gettelman and Morrison,

95   2015, hereafter as MG), which predicts mass mixing ratios and number concentrations of

96   four categories of hydrometeors: cloud droplet, cloud ice, rain, and snow. Graupel is not

97   considered in the current MG scheme. Furthermore, the MG scheme only treats the HM

98   process among various SIPs. The aerosol properties and processes are represented by the

99   four-mode version of the Model Aerosol Module (MAM4) (Liu et al., 2012, 2016). Ice

100   nucleation in cirrus clouds considers the homogeneous freezing of sulfate droplets and

101   heterogeneous freezing on dust (Liu and Penner, 2005), while the classical nucleation

102   theory (CNT) is used to treat the heterogeneous ice nucleation in mixed-phase cloud

103   regime (Wang et al., 2014; Hoose et al., 2010).

104   In our previous study (Zhao et al., 2021), we have implemented the

105   parameterizations (Phillips et al., 2017a, 2018) of the two new SIP processes: FR and IIC

106   (without graupel involved) into CAM6 via an emulated bin framework. The graupel

107   related IIC was further included in CAM6 (Zhao and Liu, 2021), with the graupel amount

108   diagnosed following Zhao et al. (2017). In this study, we compare several different ice

109   nucleation schemes in CAM6 to examine the relative importance and interactions

110   between PIP and SIP in the Arctic mixed-phase clouds.

111

112   2.2 Ice nucleation parameterization

113   CNT scheme

114   The default CAM6 uses the CNT for treating the ice nucleation in mixed-phase

115   clouds. CNT is a "stochastic" scheme which calculates the ice nucleation rates from

116   deposition, contact, and immersion freezing of cloud droplets, depending on the surface

117   areas and contact angles of cloud-borne dust and black carbon particles. The contact

118   angle is used as a proxy for the ice nucleation efficiency on INPs (Wang et al., 2014;

119   Hoose et al., 2010).

120

121   N12 scheme

122   Based on laboratory measurements from the Aerosol Interaction and Dynamics in

123   the Atmosphere (AIDA) cloud chamber, Niemand et al. (2012) (hereafter as N12)

124   proposed a surface-active site density-based scheme for the immersion freezing of cloud

125   droplets on dust aerosols. N12 is an empirical scheme that connects the dust INP number

126   concentration to the density of ice-active surface sites ($n_s(T)$) at a given temperature T,

127   total number concentration of dust aerosols (N_{tot}), and dust particle surface area (S_{ae}).

128   The dust INP number concentration in N12 is calculated as:

129     $$N_{INP}(T) = N_{tot}S_{ae}n_s(T) \qquad (1)$$

130   in which S_{ae} is calculated based on the dry diameter of dust particles, and $n_s(T)$ is

131   calculated following:

132     $$n_s(T) = e^{(-0.517(T-273.15)+8.934)} \qquad (2)$$

133

134   **D15 scheme**

135   An empirical scheme for the immersion freezing of cloud droplets on dust aerosols

136   was developed by considering dust particles with sizes larger than 0.5 μm (DeMott et al.,

137   2015), hereafter referred to as D15. This scheme argues that dust particles smaller than

138   0.5 μm may not be efficient INPs (DeMott et al., 2010, 2015). The dust INP number

139   concentration in D15 is calculated as:

140     $$N_{INP}(T) = a(n_{0.5})^b e^{c(T-273.15)-d} \qquad (3)$$

141   in which $n_{0.5}$ is the number concentration of dust particles with diameters larger than 0.5

142   μm, and the parameters $a = 3$, $b = 1.25$, $c = -0.46$, and $d = 11.6$.

143

144 **B53 scheme**

145   Bigg (1953) proposed a volume-dependent immersion freezing scheme, hereafter

146 referred to as the B53 scheme. In this scheme, the number concentration of frozen cloud

147 droplets with a diameter D is given as:

148
$$\frac{\partial N_{B53}}{\partial t} = N_c(D) \times \left(-B \times \left(e^{A \times (T_0 - T)} - 1\right) \times \frac{\pi D^3}{6}\right)$$
(4)

149 in which $\frac{\partial N_{B53}}{\partial t}$ is the ice number production rate, T is the environmental temperature in

150 unit of K, $T_0 = 273.15$ K, $A = 0.66$ and $B = 100$, and $N_c(D)$ is the number concentration

151 of cloud droplets with a diameter D.

152

153 **M92 scheme**

154   An empirical temperature dependent scheme was developed based on measurements

155 in the Northern Hemisphere midlatitudes by using a continuous-flow diffusion chamber

156 (CFDC) (Meyers et al., 1992), hereafter referred to as M92. The INP number

157 concentration is calculated as:

158
$$N_{INP} = e^{a + b \times (100 \times (S_i - 1))}$$
(5)

159 in which $a = -0.639$, $b = 0.1296$, and S_i is the saturation ratio with respect to ice.

160

161 # 3 Model setup, experiments, and observations

162   The CAM6 model was set up with the Single Column Atmospheric Model (SCAM)

163 configuration. SCAM is an efficient approach to understand the physical processes in the

164   model without the impact from nonlinear interactions with dynamic processes (Gettelman

165   et al., 2019a). In SCAM, aerosols are initialized with a monthly averaged profile for the

166   given location, which is derived from a present-day CAM6 climatological simulation.

167   Aerosol processes are fully represented in SCAM, including emission, transport,

168   chemistry, dry and wet scavenging, and aerosol-radiation and aerosol-cloud interactions

169   (Liu et al., 2012; 2016). For example, the interstitial aerosols will be activated to become

170   the cloud-borne aerosols once cloud droplets are nucleated in the cloud microphysics.

171   The cloud-borne aerosols will be released to the interstitial aerosols once cloud droplets

172   evaporate. The simulated aerosols are relaxed to a monthly averaged profile, and

173   temperature and horizontal winds to the large-scale forcing data every three hours. More

174   details about the model setup and the large-scale forcing data used to drive the model

175   experiments can be found in Zhao et al. (2021).

176   This study focuses on the Arctic mixed-phase clouds observed during the

177   Department of Energy (DOE)'s Atmospheric Radiation Program (ARM) Mixed-Phase

178   Arctic Cloud Experiment (M-PACE), which was conducted in the North Slope of Alaska

179   in October 2004 (Verlinde et al., 2007). Four major cloud regimes were identified during

180   M-PACE, i.e., the multilayer stratiform cloud period (6 to 8 October 2004), the single-

181   layer boundary-layer stratiform cloud period (9 to 12 October), the transition cloud

182   period (16 October), and the frontal cloud period (18 to 20 October).

183   Several SCAM model experiments are conducted in this study (Table 1), covering

184   the whole M-PACE period from 5 to 22 October 2004. The CNT experiment uses the

185   default CAM6 model with the MG scheme, in which only HM is considered for SIP. The

186   ice nucleation is treated by the CNT scheme. The N12, D15, B53, and M92 experiments

187   are the same as the CNT experiment except using the respective ice nucleation scheme to

188   replace the CNT scheme (section 2.2). The impacts of other SIP mechanisms rather than

189   HM, i.e., FR and IIC, are addressed in the CNT_SIP experiment. To evaluate the SIP

190   sensitivity to ice nucleation, four additional experiments with different ice nucleation

191   schemes are conducted, and these experiments are named as N12_SIP, D15_SIP,

192   B53_SIP, and M92_SIP.

193   The model simulations are compared against the M-PACE observations. The

194   observed ice water path (IWP) and liquid water path (LWP) data are from Zhao et al.

195   (2012) with uncertainties within one order of magnitude. The INP concentrations were

196   measured by a CFDC on board an aircraft (Prenni et al., 2007). McFarquhar et al. (2007)

197   documented the measured ICNCs and cloud phase during M-PACE. However, the ICNCs

198   were measured before anti-shattering algorithms were developed to remove the shattered

199   particles for the 2DC cloud probe. To remove the shattering effect, the M-PACE

200   observed ICNCs were scaled by a factor of 1/4, as Jackson and McFarquhar (2014) and

201   Jackson et al. (2014) suggested an averaged reduction of ICNCs by 1–4.5 times in other

202   field campaigns which adopted the anti-shattering algorithms and also used the 2DC

203   cloud probe.

204

4 Results

4.1 Overview of modeled clouds during M-PACE

207   The simulated LWP and IWP are compared with observations in Fig. 1 and Fig. S1.

208   First, SIP processes have a varied impact on modeled LWP and IWP, depending on ice

209   nucleation. In the experiments with the CNT, N12, and D15 ice nucleation schemes,

210   simulated IWP is enhanced and LWP is reduced after considering the SIP. In the

211   experiments with the B53 and M92 schemes, however, SIP has a minimal impact on the

212   LWP/IWP. Second, the B53, B53_SIP, M92, and M92_SIP produce the largest IWP,

213   followed by CNT_SIP, N12_SIP, and D15_SIP. CNT, N12, and D15 experiments produce

214   the smallest IWP. These characteristics are also evident in the vertical profiles of LWC and

215   IWC in Fig. 2 and Fig. S2. It indicates that the B53 and M92 nucleation schemes are highly

216   efficient in forming ice; meanwhile, the SIP simulations using CNT/N12/D15 ice

217   nucleation schemes show the modest ice production capabilities. B53, B53_SIP, M92, and

218   M92_SIP experiments generate the closest IWP compared with the observation. However,

219   these four experiments also show substantially low biases of LWP (Fig. 1 and Fig. S1), and

220   the mixed-phase clouds are almost fully glaciated during the single layer stratus period.

221   Therefore, the CNT_SIP, N12_SIP, and D15_SIP experiments give the best simulation

222   results in terms of LWP and IWP during the M-PACE. Adding the SIP does not change the

223   modeled LWP/LWC and IWP/IWC with the B53 and M92 ice nucleation schemes. On the

224   contrary, SIP significantly decreases the LWP/LWC and increases the IWP/IWC with the

225   CNT, N12, and D15 ice nucleation schemes.

226

4.2 PIP and SIP importance to ice number and cloud phase

228   A comparison between INP number concentrations (N_{INPs}) and ICNCs during 9-12

229   October is shown in Fig. 3. During this period, a long-lived single-layer mixed-phase cloud

230   occurred between 800-950 hPa, with observed cloud top temperatures of –17°C (Verlinde

231   et al., 2007). Modeled ICNCs include ice crystals of all sizes, since our purpose here is to

232   compare N_{INPs} with ICNCs. With the empirical ice nucleation schemes (e.g., N12 and

233   D15), there appears an inversely linear relationship between $\log_{10}(N_{INPs})$ and temperature

234   (Fig. 3c, d). However, this relationship is not as clear with the CNT and B53 schemes, and

235   N_{INPs} reduces dramatically at temperatures warmer than -15 ºC (Fig. 3b, e). In contrast,

236   N_{INPs} with the aerosol-independent M92 scheme is less variable with temperature, and is

237   much higher than that with the aerosol-aware schemes, such as CNT, N12, and D15,

238   particularly at warmer temperatures. We note that the model may significantly

239   underestimate dust burdens in the Arctic regions by 1-2 orders of magnitude (Shi and Liu,

240   2019) and may miss the representation of other INP sources in the Arctic (e.g., local high-

241   latitude dust, marine and terrestrial biological aerosols).

242   The ice multiplication from the SIP processes can be noted by the results that modeled

243   ICNCs are higher than modeled N_{INPs} in Fig. 3, even when we account for the 1-2 orders of

244   magnitude underestimation of N_{INPs} for these aerosol-aware ice nucleation schemes (CNT,

245   N12 and D15). The model simulation with the aerosol-independent nucleation scheme M92

246   is an exception (Fig. 3f). However, M92, which was based on the measurements in the

247   Northern Hemisphere mid-latitudes may overestimate the N_{INPs} in the Arctic during the M-

248   PACE (Prenni et al., 2007) (comparing N_{INPs} in Fig. 3a, f). Observed N_{INPs} are mostly

249   within the medium range of observed ICNCs (Fig. 3a). However, observed ICNCs only

250   include ice crystals with diameters larger than 100 μm, and thus the actual ambient ICNCs

251   including all-size ice crystals can be much higher.

252   Figure 4 shows the vertical distribution of ICNCs in the single-layer mixed-phase

253   clouds during October 9 to 12 from model simulations and observations. Here, modeled

254   and observed ICNCs only include ice particles with diameters larger than 100 μm. The

255   observed ICNCs, which range mainly between 0.1 and 1 L^{-1}, show a slight decrease with

256   altitude. CNT, N12, and D15 all show rather constant ICNCs with altitude, which are also

257   one order of magnitude lower than the observation. The ICNCs with B53 and M92 are

258   increased compared with CNT, but the vertical ICNC patterns show increasing trends with

259   altitude. As suggested in Morrison et al. (2012), the long-lived Arctic mixed-phase clouds

260   are featured with liquid phase at cloud top and ice phase at cloud bottom. The SIP

261   experiments with CNT, N12, and D15 increase the ICNCs mainly in the lower portion of

262   clouds, and thus improve the agreement with the observed vertical distribution trend of

263   ICNCs. In contrast, SIP does little changes to the ICNCs when the B53 and M92 schemes

264   are used.

265   The ICNC in the CNT experiment and ice enhancement ratios of ICNC from the other

266   experiments to that from CNT are shown in Fig. 5. The enhancement ratios are around 1.0

267   in the N12 and D15 experiments, suggesting that these three ice nucleation schemes (CNT,

268   N12, and D15) produce similar magnitudes of ICNCs, even though the N12 experiment has

269   a slightly higher ice enhancement ratio compared with the D15 experiment.

270   Correspondingly, the ice enhancement ratio patterns in the CNT_SIP, N12_SIP, and

271   D15_SIP experiments show the dominant role of SIP in increasing the ICNCs by up to 4

272   orders of magnitude. In contrast, the ice enhancement ratios in B53 and M92 are up to 3.4

273   and 4 orders of magnitude, respectively, suggesting that the B53 and M92 schemes are

274   much more efficient in producing ice particles than CNT, N12, and D15. The ice

275   enhancements in B53_SIP and M92_SIP are mainly contributed from the ice nucleation

276   (B53 and M92) with only a minor contribution from SIP, unlike the N12_SIP and D15_SIP

277   experiments where the ice enhancements are predominantly contributed from SIP.

278   Figure 6 shows the vertical distribution of the supercooled liquid fraction (SLF)

279   (defined as LWC/TWC, TWC = LWC + IWC) in the single-layer mixed-phase clouds

280   during October 9 to 12 from aircraft observations and model simulations. The CNT, N12,

281   and D15 experiments share the similar cloud phase distribution and all overestimate the

282   SLF in the lower portion of clouds. On the contrary, the B53 and M92 experiments with

283   more efficient ice nucleation show predominantly ice phase clouds, which agrees with

284   previous findings (Liu et al., 2011). The experiments with SIP (CNT_SIP, N12_SIP, and

285   D15_SIP) improve the simulated cloud phase by reducing the SLF in the CNT, N12, and

286   D15 experiments, respectively, and the SLF patterns are also similar among these

287   experiments. SIP transforms ~30% of pure liquid-phase clouds simulated in the CNT, N12,

288   and D15 experiments into mixed-phase clouds. SIP does little changes to the cloud phase

289   simulated in the B53_SIP and M92_SIP experiments, since the clouds are already glaciated

290   by ice crystals nucleated with the B53 and M92 schemes. These findings highlight that the

291   "foundation" effect of PIP on the cloud phase. We note that the CNT_SIP, N12_SIP, and

292   D15_SIP experiments overall have the best performance in terms of vertical distribution of

293   ICNCs and cloud phase during the single-layer mixed-phase cloud period.

294   Figure 7 show the relative contributions from PIP and SIP processes to the total ice

295   production from model experiments with different ice nucleation schemes averaged over

296   different M-PACE periods. We notice that the CNT_SIP, N12_SIP, and D15_SIP

297   experiments have similar relative contributions between PIP and SIP. The averaged PIP

298   contribution is around 20% for all the cloud types observed during M-PACE, with the

299   maximum contribution of 60% for the frontal clouds, and the minimum contribution of 7%

300   for the single-layer mixed-phase clouds. Moreover, the IIC is the dominant ice production

301   process in these three experiments, with an averaged contribution of 60%. On the contrary,

302   the B53_SIP and M92_SIP experiments show much larger contributions from PIP, which

303   contributes 65% and 80% to the total ice production, respectively averaged for all the cloud

304   types. However, we note that the unrealistic pure ice-phase clouds simulated in the B53

305   and M92 experiments imply that the role of ice nucleation in these experiments is

306   overstated. Given that the CNT_SIP, N12_SIP, and D15_SIP experiments give the best

307   performance in simulating ICNCs and cloud phase, their estimates of the relative

308   importance of primary and secondary ice production are more reliable.

309

310   4.3 Interactions between PIP and SIP

311   Figure 8 shows the temporally-averaged vertical profiles of PIP and SIP process rates

312   and total from experiments with the CNT and M92 ice nucleation schemes, respectively

313   during the single-layer mixed-phase cloud period (October 9 to 12). As shown in Fig. 8a,

314   clear suppression of PIP by SIP is revealed: the ice nucleation rate is reduced after the SIP

315   is introduced for both CNT and M92 ice nucleation but with different sensitivities. The

316   M92 ice nucleation is more suppressed by SIP than the CNT ice nucleation. The peak PIP

317   rate is reduced by about one order of magnitude in M92 compared to a factor of 2 in CNT.

318   The suppression of PIP by SIP is robust for the other three ice nucleation schemes over the

319   single-layer mixed-phase cloud period (Fig. S4), as well as for the whole M-PACE period

320   (Figs. S5 and S6).

321  The mechanism for the suppression of PIP by SIP for the CNT ice nucleation is

322 illustrated in Figure 9. The ice nucleation is contributed from heterogeneous immersion,

323 deposition and contact ice nucleation. Among these mechanisms, the immersion freezing is

324 the dominant process in the single-layer mixed-phase clouds (Fig. 9a, b, c). The immersion

325 freezing rate is a function of INPs in cloud droplets and temperature. CNT calculates the

326 immersion freezing rate based on cloud-borne black carbon and dust, the latter of which is

327 the dominant INPs.

328  The immersion ice nucleation is substantially weakened (Fig. 9a) after considering

329 SIP in the model due to lower number concentrations of INPs (Fig. 9d) and cloud droplets

330 (Fig. 9g). The cloud-borne dust number concentrations in the accumulation (Fig. 9e) and

331 coarse modes (Fig. 9f) are both decreased below ~750 hPa level, corresponding to the

332 reduction of INP number concentration and immersion ice nucleation rate in CNT_SIP

333 compared to the CNT experiment. Lower cloud-borne dust number concentrations in the

334 CNT_SIP experiment are caused by the reduction of cloud droplet number concentrations

335 (Fig. 9g) as a result of SIP. The SIP strongly enhances the accretion of cloud water by snow

336 (Fig. 9h) and the WBF process (Fig. 9i), leading to more consumption of cloud water (Zhao

337 and Liu, 2021).

338  The N12 and D15 schemes calculate the INP number concentrations based on the

339 interstitial aerosols (section 2.2). The mechanism for the suppression of PIP by SIP in the

340 case of the N12 ice nucleation is shown in Fig. S7: less cloud droplets and less available

341   interstitial aerosols (as a result of stronger wet deposition) with the introduction of SIP lead

342   to weaker PIP. The B53 and M92 schemes calculate the ice nucleation based on

343   temperature, supersaturation, and cloud droplet number concentration (section 2.2). Since

344   temperature and supersaturation are similar in these nudged experiments, the decreased

345   cloud droplet number concentration with the introduction of SIP leads to weaker PIP in

346   B53_SIP and M92_SIP.

347   On the other hand, ice nucleation can also compete with SIP. The ice nucleation

348   scheme with a larger ice nucleation rate (e.g., M92 versus CNT, Fig. 8a) is in accompany

349   with a smaller SIP rate (Fig. 8b). The peak SIP rate in M92_SIP is ~10^{-14} kg kg^{-1} s^{-1}, which

350   is about 10 times lower than that in CNT_SIP (~10^{-13} kg kg^{-1} s^{-1}). This competition

351   between PIP and SIP is also revealed in the other ice nucleation schemes for the single-

352   layer mixed-phase cloud period (Fig. S4) and for the whole M-PACE period (Figs. S5 and

353   S6). We note that the largest PIP rate is M92, followed by B53, CNT, N12, and D15, while

354   the SIP rate is in the reversed order.

355   The mechanism for the suppression of SIP by PIP is illustrated in Figure 10. First, the

356   SIP rate is determined by three components, FR, IIC, and HM (Fig. 10a, b, c). The SIP rate

357   is dominated by IIC and FR. Second, the smaller FR rate in M92_SIP compared to that in

358   CNT_SIP (Fig. 10a) is a result of smaller rainwater mass mixing ratio (Fig. 10d), which is

359   caused by the strong M92 ice nucleation resulting in nearly complete glaciation of the

360   cloud in the M92_SIP experiment. Third, the IIC can be further subdivided into the non-

361   graupel-related IIC (Fig. 10e) and the graupel-related IIC (Fig. 10f), the latter of which

362   dominates the total IIC. A smaller graupel-related IIC rate (Fig. 10f) in M92_SIP compared

363   to CNT_SIP is a result of smaller graupel mass mixing ratio in M92_SIP (Fig. 10g). As the

364   graupel mass is diagnosed from the cloud water mass, snow mass, and temperature, smaller

365   mass mixing ratios of cloud water (Fig. 10h) and snow (Fig. 10i) in M92_SIP eventually

366   lead to a smaller graupel mass mixing ratio and a smaller graupel-related IIC rate. Similar

367   results can be found with the other ice nucleation schemes.

368   In summary, different from the PIP rate which is dependent on cloud-borne aerosols

369   and cloud droplets, the SIP rate is directly controlled by the precipitation particles, such as

370   rain, snow, and graupel. A stronger ice nucleation leads to more glaciation of mixed-phase

371   clouds in M92_SIP. As a consequence, less rainwater and graupel exist, leading to lower

372   SIP rate in the M92_SIP experiment compared to the CNT experiment.

373

374   5 Summary and conclusions

375   In this study, the relative importance of PIP through ice nucleation and SIP and their

376   interactions are investigated for the Arctic single-layer mixed-phase clouds observed

377   during M-PACE. To understand the interactions between PIP and SIP, five different ice

378   nucleation schemes (CNT, N12, D15, B53 and M92) are implemented in the model.

379   Model experiments with only ice nucleation and with both ice nucleation and SIP are

380   conducted. The CNT, N12, and D15 experiments without considering SIP show rather

381   constant ICNCs with cloud height, which are also one order of magnitude lower than the

382   observation. The SIP experiments based on the CNT, N12 and D15 ice nucleation schemes

383   (i.e., CNT_SIP, N12_SIP, and D15_SIP) reverse the vertical distribution pattern of ICNCs

384   by increasing the ICNCs in the lower portion of clouds. SIP also transforms ~30% of pure

385   liquid-phase clouds simulated in the CNT, N12, and D15 experiments into mixed-phase

386   clouds. In contrast, modeled clouds are totally ice phase instead of observed mixed-phase

387   in the B53 and M92 experiments. Since the cloud is already completely glaciated by the ice

388   nucleation with these ice nucleation schemes, adding the SIP processes has little impact on

389   the cloud phase in the B53_SIP and M92_SIP experiments. These findings highlight the

390   "foundation" effect of PIP on the cloud phase. We conclude that the model experiments

391   with both aerosol-aware ice nucleation schemes and SIP processes (i.e., CNT_SIP,

392   N12_SIP, and D15_SIP) yield the best agreement with observations in simulating the

393   Arctic single-layer mixed-phase clouds.

394   The relative importance of PIP and SIP is investigated in this study. We find that ice

395   nucleation contributes around 20% to the total ice production during M-PACE, with a

396   maximum value of 60% for the frontal clouds, and a minimum value of 7% for the single-

397   layer mixed-phase clouds in the CNT_SIP, N12_SIP, and D15_SIP experiments. The

398   B53_SIP and M92_SIP experiments may overestimate the contribution from PIP, which

399   contributes 65% and 80% to the total ice production, respectively averaged over the M-

400   PACE clouds.

401   In this study, for the first time, the interactions between PIP and SIP in the single-

402   layer mixed-phase clouds are investigated and possible mechanisms behind are discussed.

403   We find a clear suppression of PIP by SIP, and the ice nucleation rate is reduced when SIP

404   is introduced in the model. Ice crystals produced from SIP trigger a series of changes in

405   microphysical processes (e.g., WBF, riming), resulting in reduced number concentrations

406   of cloud droplets and cloud-borne dust aerosols. Less cloud-borne dust aerosols eventually

407   cause a weakening of the following ice nucleation (e.g., immersion freezing of cloud

408   droplets on dust). On the other hand, ice nucleation also competes with SIP. The ice

409   nucleation schemes with larger nucleation rates are in accompany with smaller SIP rates.

410   Different from the ice nucleation which depends on cloud water and aerosols, the SIP rate

411   is directly controlled by the precipitation particles. A stronger ice nucleation leads to more

412   glaciation of mixed-phase clouds, and as a consequence, less rain and graupel are formed,

413   leading to lower SIP rate.

414   We note that uncertainties still exist in the representations of ice nucleation and SIP in

415   the model. First, the diagnostic graupel approach still has a large uncertainty. A cloud

416   microphysical scheme with prognostic graupel (Gettelman et al., 2019b) or a "Single-Ice"

417   microphysical scheme (Morrison and Milbrandt, 2015; Zhao et al., 2017) will be needed to

418   further examine the impacts of graupel-related IIC. Second, modeled INP concentrations

419   may be significantly underestimated in the Arctic regions with the aerosol-aware CNT,

420   D15, and N12 ice nucleation schemes. This is owing to the model underestimation of long-

421   range transport of dust from lower latitudes as well as the model missing of high-latitude

422   local dust and biological aerosol emissions in the Arctic regions. The underestimation of

423   modeled INPs can reach 1-2 orders of magnitude (Shi and Liu, 2019; Shi et al., 2021). A

424   sensitivity test using CNT scheme with 100 times dust concentration shows overall similar

425   cloud properties, but the relative contribution of primary ice nucleation is increased by 1~2

426   times. Our future work will focus on representing the high latitude dust and biological

427   aerosol emissions in the model as well as improving the parameterization of SIP processes.

428

429   **Competing interests:** The authors declare that they have no conflict of interest.

430

431   **Data availability:** The Community Earth System Model version 2 (CESM) source code is

432   freely available at http://www. cesm.ucar.edu/models/cesm2 (Danabasoglu et al., 2020;

433   last access: 3 July 2021). The SIP source code and model datasets are archived at the NCAR

434   Cheyenne supercomputer and are available upon request. The measured LWP and IWP

435   datasets of M-PACE campaign are obtained from the Atmospheric Radiation Measurement

436   (ARM) user facility, US Department of Energy Office of Science, available at

437   https://www.arm.gov/research/campaigns/nsa2004arcticcld (McFarquhar et al., 2007; last

438   access: 3 July 2021).

439

440 **Author contributions**: XZ and XL conceptualized the analysis,carried out the simulations,

441 performed the analysis, and wrote the manuscript. XL was involved with obtaining the

442 project grant and supervised the study.

443

444 **Acknowledgment:** We thank Vaughan T. J. Phillips, and Sachin Patade for helpful

445 discussions. We thank Meng Zhang for helpful discussions, especially on processing the

446 observation data. The authors would also like to acknowledge the use of computational

447 resources for conducting the model simulations (ark:/85065/d7wd3xhc) at the NCAR-

448 Wyoming Supercomputing Center provided by the NSF and the State of Wyoming and

449 supported by NCAR's Computational and Information Systems Laboratory.

450

451 **Financial support:** This research was supported by the DOE Atmospheric System

452 Research (ASR) Program (grants DE-SC0020510 and DE-SC0021211).

References

Atkinson, J. D., Murray, B. J., Woodhouse, M. T., Whale, T. F., Baustian, K. J., Carslaw, K. S., Dobbie, S., O'Sullivan, D., and Malkin, T. L.: The importance of feldspar for ice nucleation by mineral dust in mixed-phase clouds, Nature 2013 498:7454, 498, 355-358, 10.1038/nature12278, 2013.

Beard, K. V.: Ice initiation in warm-base convective clouds: An assessment of microphysical mechanisms, Atmospheric Research, 28, 125-152, 10.1016/0169-8095(92)90024-5, 1992.

Bigg, E. K.: The Supercooling of Water, P Phys Soc Lond B, 66, 688-694, Doi 10.1088/0370-1301/66/8/309, 1953.

Crawford, I., Bower, K. N., Choularton, T. W., Dearden, C., Crosier, J., Westbrook, C., Capes, G., Coe, H., Connolly, P. J., Dorsey, J. R., Gallagher, M. W., Williams, P., Trembath, J., Cui, Z., and Blyth, A.: Ice formation and development in aged, wintertime cumulus over the UK: observations and modelling, Atmos Chem Phys, 12, 4963-4985, 10.5194/acp-12-4963-2012, 2012.

Danabasoglu, G., Lamarque, J. F., Bacmeister, J., Bailey, D. A., DuVivier, A. K., Edwards, J., Emmons, L. K., Fasullo, J., Garcia, R., Gettelman, A., Hannay, C., Holland, M. M., Large, W. G., Lauritzen, P. H., Lawrence, D. M., Lenaerts, J. T. M., Lindsay, K., Lipscomb, W. H., Mills, M. J., Neale, R., Oleson, K. W., Otto-Bliesner, B., Phillips, A. S., Sacks, W., Tilmes, S., van Kampenhout, L., Vertenstein, M., Bertini, A., Dennis, J., Deser, C., Fischer, C., Fox-Kemper, B., Kay, J. E., Kinnison, D., Kushner, P. J., Larson, V. E., Long, M. C., Mickelson, S., Moore, J. K., Nienhouse, E., Polvani, L., Rasch, P. J., and Strand, W. G.: The Community Earth System Model Version 2 (CESM2), Journal of Advances in Modeling Earth Systems, 12, e2019MS001916, 10.1029/2019MS001916, 2020.

DeMott, P. J., Prenni, A. J., Liu, X., Kreidenweis, S. M., Petters, M. D., Twohy, C. H., Richardson, M. S., Eidhammer, T. and Rogers, D. C.: Predicting global atmospheric ice nuclei distributions and their impacts on climate, Proceedings of the National Academy of Sciences of the United States of America, 107(25), 11217–11222, https://doi.org/10.1073/pnas.0910818107, 2010.

DeMott, P. J., Prenni, A. J., McMeeking, G. R., Sullivan, R. C., Petters, M. D., Tobo, Y., Niemand, M., Mohler, O., Snider, J. R., Wang, Z., and Kreidenweis, S. M.:

485   Integrating laboratory and field data to quantify the immersion freezing ice

486   nucleation activity of mineral dust particles, Atmos Chem Phys, 15, 393-409, 2015.

487   Field, P. R., Lawson, R. P., Brown, P. R. A., Lloyd, G., Westbrook, C., Moisseev, D.,

488   Miltenberger, A., Nenes, A., Blyth, A., Choularton, T., Connolly, P., Buehl, J.,

489   Crosier, J., Cui, Z., Dearden, C., DeMott, P., Flossmann, A., Heymsfield, A., Huang,

490   Y., Kalesse, H., Kanji, Z. A., Korolev, A., Kirchgaessner, A., Lasher-Trapp, S.,

491   Leisner, T., McFarquhar, G., Phillips, V., Stith, J., and Sullivan, S.: Chapter 7.

492   Secondary Ice Production - current state of the science and recommendations for the

493   future, Meteorological Monographs, 58, 7.1-7.20, 10.1175/amsmonographs-d-16-

494   0014.1, 2017.

495   Gettelman, A., and Morrison, H.: Advanced two-moment bulk microphysics for global

496   models. Part I: Off-line tests and comparison with other schemes, Journal of

497   Climate, 28, 1268-1287, 10.1175/JCLI-D-14-00102.1, 2015.

498   Gettelman, A., Truesdale, J. E., Bacmeister, J. T., Caldwell, P. M., Neale, R. B.,

499   Bogenschutz, P. A., and Simpson, I. R.: The Single Column Atmosphere Model

500   Version 6 (SCAM6): Not a Scam but a Tool for Model Evaluation and

501   Development, Journal of Advances in Modeling Earth Systems, 11, 1381-1401,

502   10.1029/2018MS001578, 2019a.

503   Gettelman, A., Morrison, H., Thayer-Calder, K. and Zarzycki, C. M.: The Impact of

504   Rimed Ice Hydrometeors on Global and Regional Climate, Journal of Advances in

505   Modeling Earth Systems, 11(6), 1543–1562,

506   https://doi.org/10.1029/2018MS001488, 2019b.

507   Hoose, C., Kristjánsson, J. E., Chen, J. P., and Hazra, A.: A classical-theory-based

508   parameterization of heterogeneous ice nucleation by mineral dust, soot, and

509   biological particles in a global climate model, Journal of the Atmospheric Sciences,

510   67, 2483-2503, 10.1175/2010JAS3425.1, 2010.

511   Hoose, C., Lohmann, U., Erdin, R., and Tegen, I.: The global influence of dust

512   mineralogical composition on heterogeneous ice nucleation in mixed-phase clouds,

513   Environ Res Lett, 3, 025003, 10.1088/1748-9326/3/2/025003, 2008.

514   Huang, Y., Blyth, A. M., Brown, P. R. A., Choularton, T. W., and Cui, Z.: Factors

515   controlling secondary ice production in cumulus clouds, Q J Roy Meteor Soc, 143,

516   1021-1031, 10.1002/qj.2987, 2017.

517   Jackson, R. C., and McFarquhar, G. M.: An assessment of the impact of antishattering

518   tips and artifact removal techniques on bulk cloud ice microphysical and optical

519   properties measured by the 2D cloud probe, J Atmos Ocean Tech, 31, 2131-2144,
520   10.1175/JTECH-D-14-00018.1, 2014.

521   Jackson, R. C., Mcfarquhar, G. M., Stith, J., Beals, M., Shaw, R. A., Jensen, J., Fugal, J.,
522   and Korolev, A.: An assessment of the impact of antishattering tips and artifact
523   removal techniques on cloud ice size distributions measured by the 2D cloud probe,
524   J Atmos Ocean Tech, 31, 2567-2590, 10.1175/JTECH-D-13-00239.1, 2014.

525   Kanji, Z. A., Ladino, L. A., Wex, H., Boose, Y., Burkert-Kohn, M., Cziczo, D. J., and
526   Krämer, M.: Overview of Ice Nucleating Particles, Meteorological Monographs, 58,
527   1.1-1.33, 10.1175/amsmonographs-d-16-0006.1, 2017.

528   Korolev, A., and Isaac, G.: Phase transformation of mixed-phase clouds, Q J Roy Meteor
529   Soc, 129, 19-38, 10.1256/QJ.01.203, 2003.

530   Korolev, A., and Leisner, T.: Review of experimental studies of secondary ice
531   production, Atmos Chem Phys, 20, 11767-11797, 10.5194/acp-20-11767-2020,
532   2020.

533   Korolev, A., McFarquhar, G., Field, P. R., Franklin, C., Lawson, P., Wang, Z., Williams,
534   E., Abel, S. J., Axisa, D., Borrmann, S., Crosier, J., Fugal, J., Krämer, M., Lohmann,
535   U., Schlenczek, O., Schnaiter, M., and Wendisch, M.: Mixed-Phase Clouds:
536   Progress and Challenges, Meteorological Monographs, 58, 5.1-5.50,
537   10.1175/amsmonographs-d-17-0001.1, 2017.

538   Lasher-Trapp, S., Leon, D. C., DeMott, P. J., Villanueva-Birriel, C. M., Johnson, A. V.,
539   Moser, D. H., Tully, C. S., and Wu, W.: A Multisensor Investigation of Rime
540   Splintering in Tropical Maritime Cumuli, Journal of the Atmospheric Sciences, 73,
541   2547-2564, 10.1175/JAS-D-15-0285.1, 2016.

542   Liu, X., Easter, R. C., Ghan, S. J., Zaveri, R., Rasch, P., Shi, X., Lamarque, J.-F.,
543   Gettelman, A., Morrison, H., Vitt, F., Conley, A., Park, S., Neale, R., Hannay, C.,
544   Ekman, A. M. L., Hess, P., Mahowald, N., Collins, W., Iacono, M. J., Bretherton, C.
545   S., Flanner, M. G., and Mitchell, D.: Toward a minimal representation of aerosols in
546   climate models: description and evaluation in the Community Atmosphere Model
547   CAM5, Geosci. Model Dev., 5, 709–739, https://doi.org/10.5194/gmd-5-709-2012,
548   2012.

549   Liu, X., Ma, P.-L., Wang, H., Tilmes, S., Singh, B., Easter, R. C., Ghan, S. J., and Rasch,
550   P. J.: Description and evaluation of a new four-mode version of the Modal Aerosol
551   Module (MAM4) within version 5.3 of the Community Atmosphere Model, Geosci.
552   Model Dev., 9, 505–522, https://doi.org/10.5194/gmd-9-505-2016, 2016.

553 Liu, X., and Penner, J. E.: Ice nucleation parameterization for global models,
554   Meteorologische Zeitschrift, 14, 499-514, 10.1127/0941-2948/2005/0059, 2005.
555 Liu, X., Xie, S., Boyle, J., Klein, S. A., Shi, X., Wang, Z., Lin, W., Ghan, S. J., Earle, M.,
556   Liu, P. S. K., and Zelenyuk, A.: Testing cloud microphysics parameterizations in
557   NCAR CAM5 with ISDAC and M-PACE observations, Journal of Geophysical
558   Research, 116, D00T11, 10.1029/2011JD015889, 2011.
559 McFarquhar, G. M., Zhang, G., Poellot, M. R., Kok, G. L., McCoy, R., Tooman, T.,
560   Fridlind, A., and Heymsfield, A. J.: Ice properties of single-layer stratocumulus
561   during the Mixed-Phase Arctic Cloud Experiment: 1. Observations, Journal of
562   Geophysical Research, 112, D24201, 10.1029/2007JD008633, 2007.
563 Meyers, M. P., Demott, P. J. and Cotton, W. R.: New primary ice-nucleation
564   parameterizations in an explicit cloud model, Journal of Applied Meteorology,
565   31(7), 708–721, https://doi.org/10.1175/1520-
566   0450(1992)031<0708:NPINPI>2.0.CO;2, 1992.
567 Morrison, H., de Boer, G., Feingold, G., Harrington, J., Shupe, M. D. and Sulia, K.:
568   Resilience of persistent Arctic mixed-phase clouds, Nature Geoscience, 5(1), 11–17,
569   https://doi.org/10.1038/ngeo1332, 2012.
570 Morrison, H. and Milbrandt, J. A.: Parameterization of cloud microphysics based on the
571   prediction of bulk ice particle properties. Part I: Scheme description and idealized
572   tests, Journal of the Atmospheric Sciences, 72(1), 287–311,
573   https://doi.org/10.1175/JAS-D-14-0065.1, 2015.
574 Mossop, S. C.: Secondary ice particle production during rime growth: The effect of drop
575   size distribution and rimer velocity, Q J Roy Meteor Soc, 111, 1113-1124,
576   10.1002/qj.49711147012, 1985.
577 Niemand, M., Möhler, O., Vogel, B., Vogel, H., Hoose, C., Connolly, P., Klein, H.,
578   Bingemer, H., DeMott, P., Skrotzki, J., and Leisner, T.: A Particle-Surface-Area-
579   Based Parameterization of Immersion Freezing on Desert Dust Particles, Journal of
580   the Atmospheric Sciences, 69, 3077-3092, 10.1175/JAS-D-11-0249.1, 2012.
581 Phillips, V. T. J., Patade, S., Gutierrez, J., and Bansemer, A.: Secondary ice production
582   by fragmentation of freezing drops: Formulation and theory, Journal of the
583   Atmospheric Sciences, 75, 3031-3070, 10.1175/JAS-D-17-0190.1, 2018.
584 Phillips, V. T. J., Yano, J. I., Formenton, M., Ilotoviz, E., Kanawade, V., Kudzotsa, I.,
585   Sun, J., Bansemer, A., Detwiler, A. G., Khain, A., and Tessendorf, S. A.: Ice
586   multiplication by breakup in ice-ice collisions. Part II: Numerical simulations,

587   Journal of the Atmospheric Sciences, 74, 2789-2811, 10.1175/JAS-D-16-0223.1,

588   2017.

589 Phillips, V. T. J., Yano, J. I., and Khain, A.: Ice multiplication by breakup in ice-ice

590   collisions. Part I: Theoretical formulation, Journal of the Atmospheric Sciences, 74,

591   1705-1719, 10.1175/JAS-D-16-0224.1, 2017.

592 Prenni, A. J., Harrington, J. Y., Tjernström, M., DeMott, P. J., Avramov, A., Long, C. N.,

593   Kreidenweis, S. M., Olsson, P. Q., and Verlinde, J.: Can Ice-Nucleating Aerosols

594   Affect Arctic Seasonal Climate?, B Am Meteorol Soc, 88, 541-550,

595   10.1175/BAMS-88-4-541, 2007.

596 Sullivan, S. C., Hoose, C., Kiselev, A., Leisner, T., and Nenes, A.: Initiation of secondary

597   ice production in clouds, Atmos Chem Phys, 18, 1593-1610, 10.5194/acp-18-1593-

598   2018, 2018.

599 Verlinde, J., Harrington, J. Y., McFarquhar, G. M., Yannuzzi, V. T., Avramov, A.,

600   Greenberg, S., Johnson, N., Zhang, G., Poellot, M. R., Mather, J. H., Turner, D. D.,

601   Eloranta, E. W., Zak, B. D., Prenni, A. J., Daniel, J. S., Kok, G. L., Tobin, D. C.,

602   Holz, R., Sassen, K., Spangenberg, D., Minnis, P., Tooman, T. P., Ivey, M. D.,

603   Richardson, S. J., Bahrmann, C. P., Shupe, M., DeMott, P. J., Heymsfield, A. J., and

604   Schofield, R.: The mixed-phase arctic cloud experiment, B Am Meteorol Soc, 88,

605   205-221, 10.1175/BAMS-88-2-205, 2007.

606 Wang, Y., Liu, X., Hoose, C., and Wang, B.: Different contact angle distributions for

607   heterogeneous ice nucleation in the Community Atmospheric Model version 5,

608   Atmos Chem Phys, 14, 10411-10430, 2014.

609 Zhao, X., Lin, Y., Peng, Y., Wang, B., Morrison, H. and Gettelman, A.: A single ice

610   approach using varying ice particle properties in global climate model microphysics,

611   Journal of Advances in Modeling Earth Systems, 9(5), 2138–2157,

612   https://doi.org/10.1002/2017MS000952, 2017.

613 Zhao, X., and Liu, X.: Global Importance of Secondary Ice Production, Geophys Res

614   Lett, e2021GL092581, 10.1029/2021GL092581, 2021.

615 Zhao, X., Liu, X., Phillips, V. T. J., and Patade, S.: Impacts of secondary ice production

616   on Arctic mixed-phase clouds based on ARM observations and CAM6 single-

617   column model simulations, Atmos Chem Phys, 21, 5685-5703, 10.5194/acp-21-

618   5685-2021, 2021.

619

tio

623

624   Figure 1. Temporal evolution of (a) LWP and (b) IWP from remote sensing retrievals

625   (symbols) and CNT, CNT_SIP, N12, N12_SIP, M92, and M92_SIP experiments (lines);

626   (c) vertical distribution of observed cloud fraction. The light orange shadings show the

627   multilayer stratus and transition periods; light blue shadings show the single-layer stratus

628   and frontal clouds periods. Note that N12 (N12_SIP) coincides with CNT (CNT_SIP)

629   during the single-layer stratus cloud period.

630

631

632
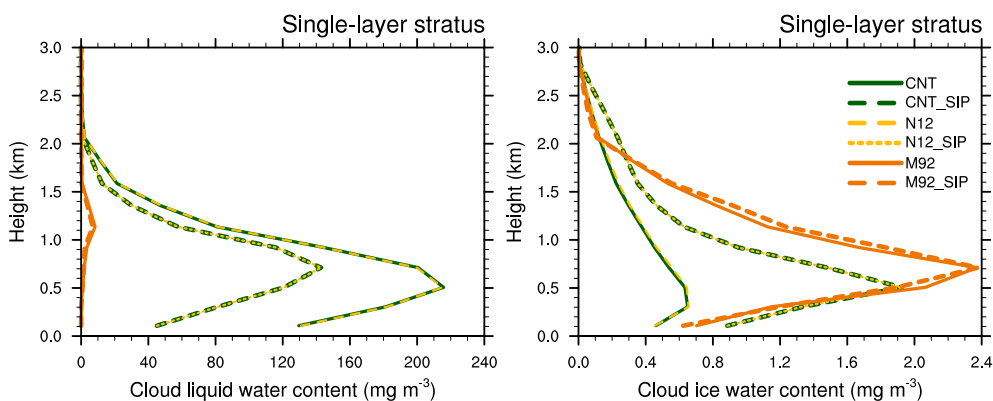
Figure 2. Vertical profiles of LWC (left) and IWC (right) during the single-layer mixed-

phased cloud period (October 9-12) from CNT, CNT_SIP, N12, N12_SIP, M92, and

M92_SIP experiments. Note that N12 (N12_SIP) coincides with CNT (CNT_SIP) during

the single layer stratus cloud period.

637

638
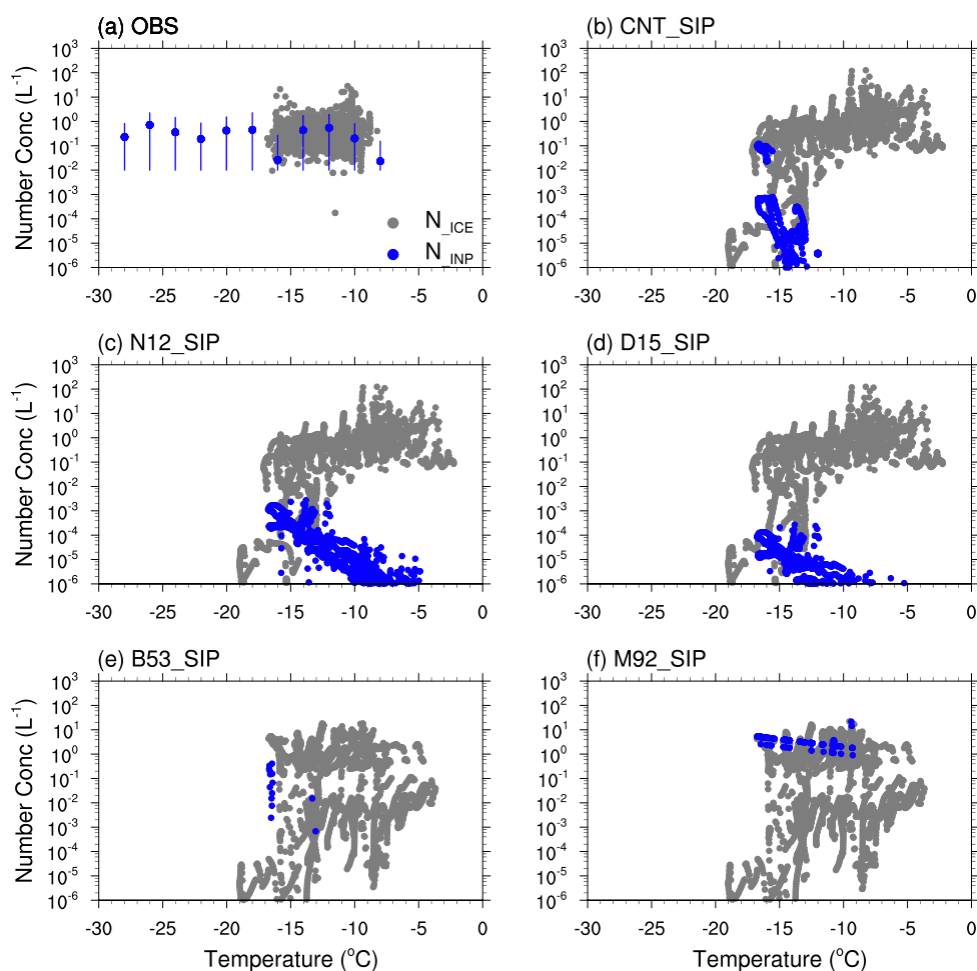
Figure 3. Comparison between INP (blue dots, in unit of L^{-1}) and ice crystal number

concentrations (gray dots, in unit of L^{-1}) from (a) observations, (b) CNT_SIP, (c)

N12_SIP, (d) D15_SIP, (e) B53_SIP, and (f) M92_SIP experiments. Modeled ice number

concentrations include ice crystals of all sizes, since the purpose of this figure is to

compare INP number concentrations with ice crystal number concentrations. To account

for the anti-shattering tip effect, only ice particles with diameters larger than 100 μm

from observations are included in Fig. 3a, and a correction factor of 1/4 is also applied to

the measured ice crystal number concentrations based on Jackson et al. (2014) and

Jackson and McFarquhar (2014).
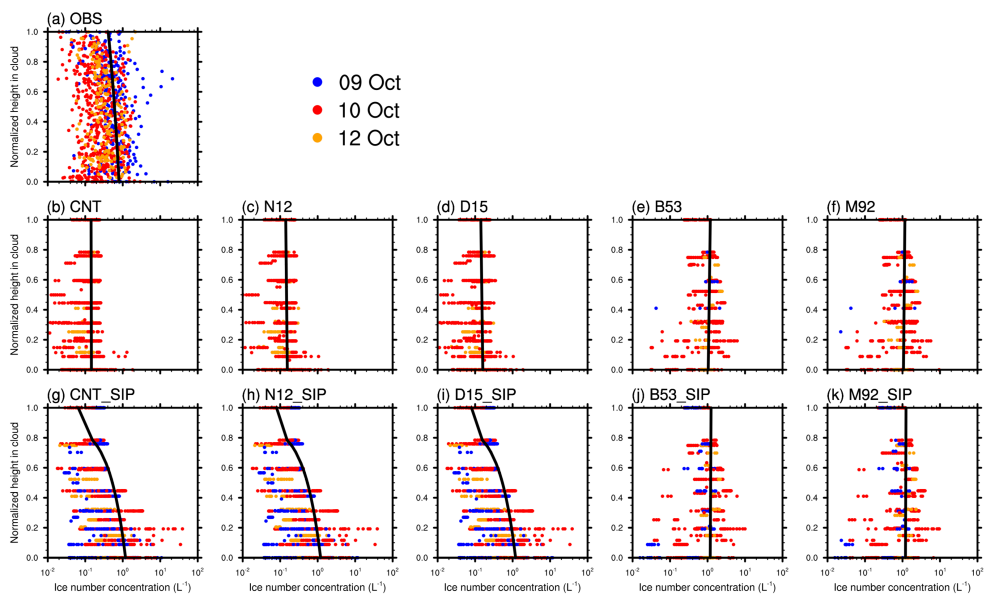
648

649   Figure 4. Ice crystal number concentrations as a function of normalized cloud height (i.e.,

650   0 for cloud base and 1 for cloud top) from (a) observation, (b) CNT, (c) N12, (d) D15, (e)

651   B53, (f) M92, (g) CNT_SIP, (h) N12_SIP, (i) D15_SIP, (j) B53_SIP, and (k) M92_SIP

652   experiments. Black solid lines show the linear regression between ice number

653   concentration and height. Only ice particles with diameters larger than 100 μm from

654   simulations and observations are included in the comparison. To account for the anti-

655   shattering tip effect, a correction factor of 1/4 is applied to the measured ice number

656   concentrations based on Jackson et al. (2014) and Jackson and McFarquhar (2014).

657

658
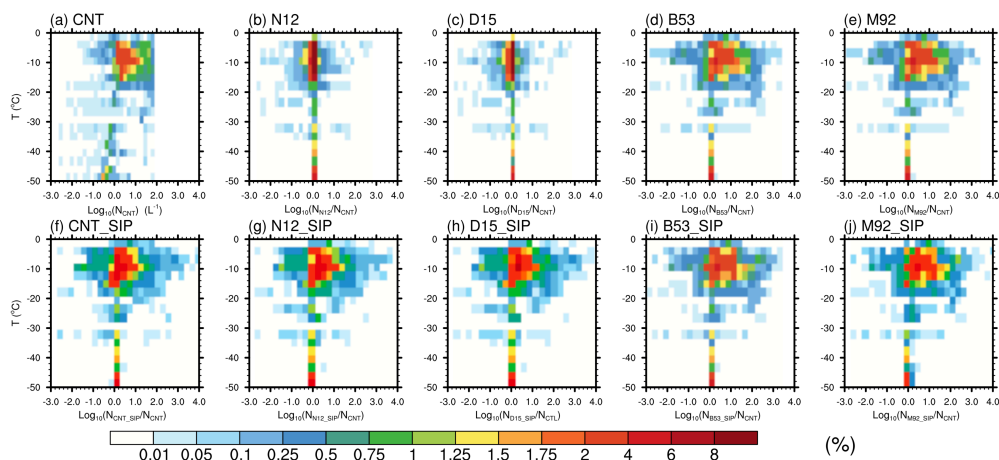
Figure 5. Bivariate joint probability density functions (PDF) of (a) ice crystal number

concentration (L^{-1}) from the CNT experiment; and (b)-(j) enhancement ratios of ice

crystal number concentration from the respective experiment to that from the CNT

experiment as a function of temperature. A logarithmic scale is used for x-axis.

663

664
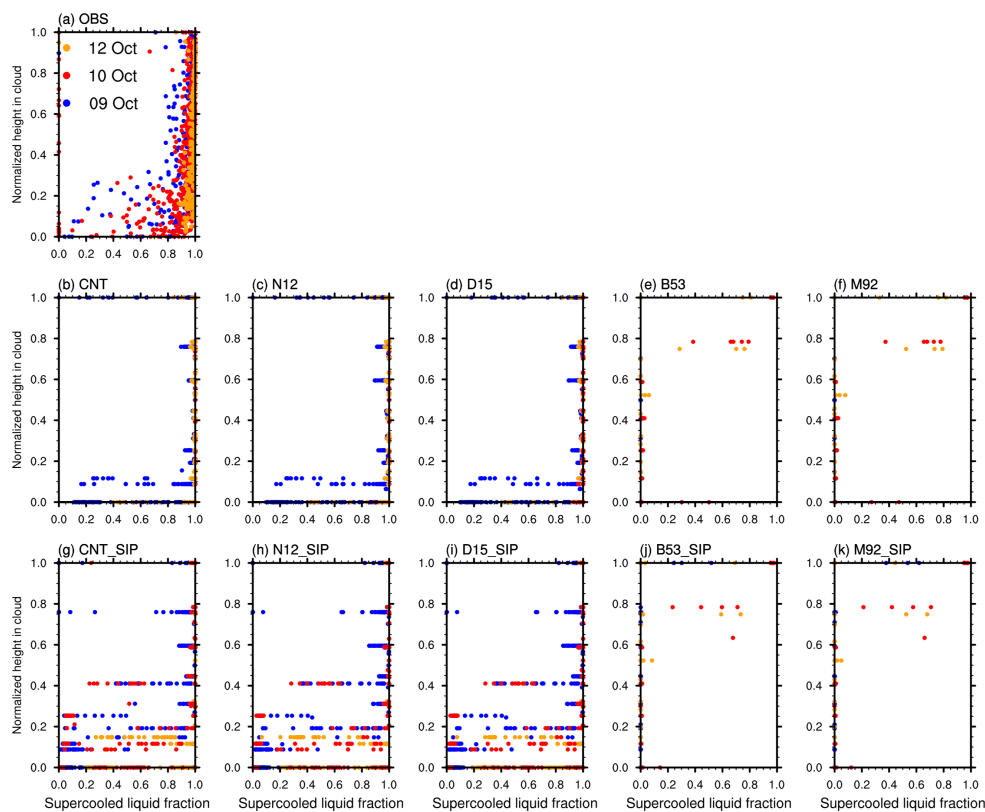
Figure 6. Supercooled liquid fraction (defined as LWC/(LWC + IWC)) as a function of

normalized cloud height (i.e., 0 for cloud base and 1 for cloud top) from observations and

model experiments.

668
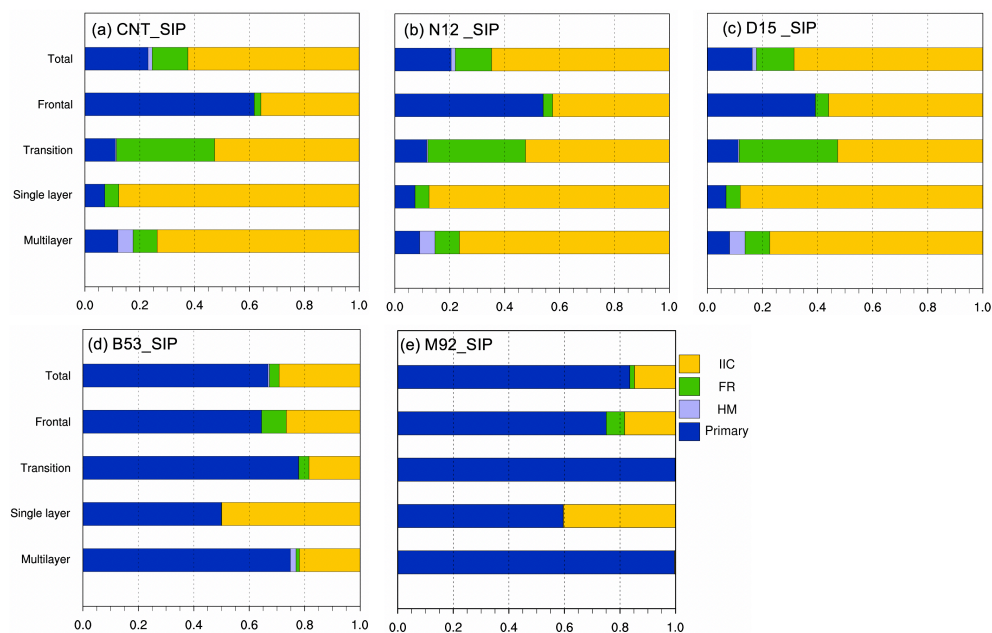
Figure 7. Stacked bar charts of relative contributions from ice nucleation and secondary ice production to the total ice production rate from (a) CNT_SIP, (b) N12_SIP, (c) D15_SIP, (d) B53_SIP, and (e) M92_SIP experiments averaged over different time periods of M-PACE. The secondary ice production includes ice-ice collisional breakup (IIC), rain droplet fragmentation (FR), and Hallett–Mossop (HM) process.
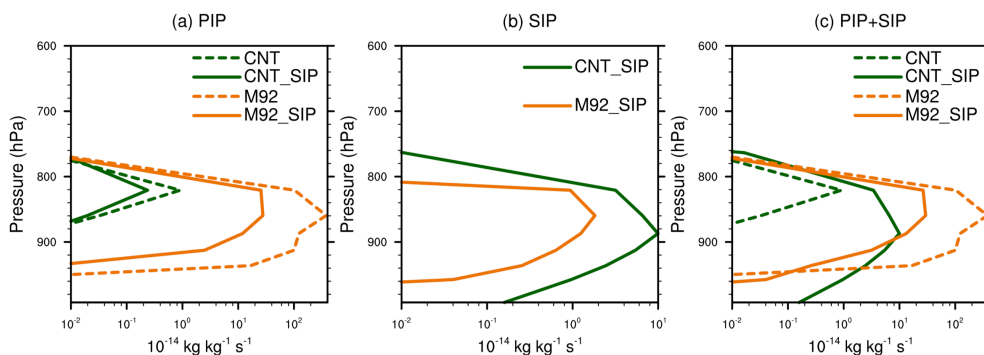
Figure 8. Vertical profiles of (a) primary ice production rate, (b) secondary ice production rate, and (c) primary plus secondary ice production rate from CNT, CNT_SIP, M92, and M92_SIP model experiments averaged over the single-layer mixed-phase cloud period.
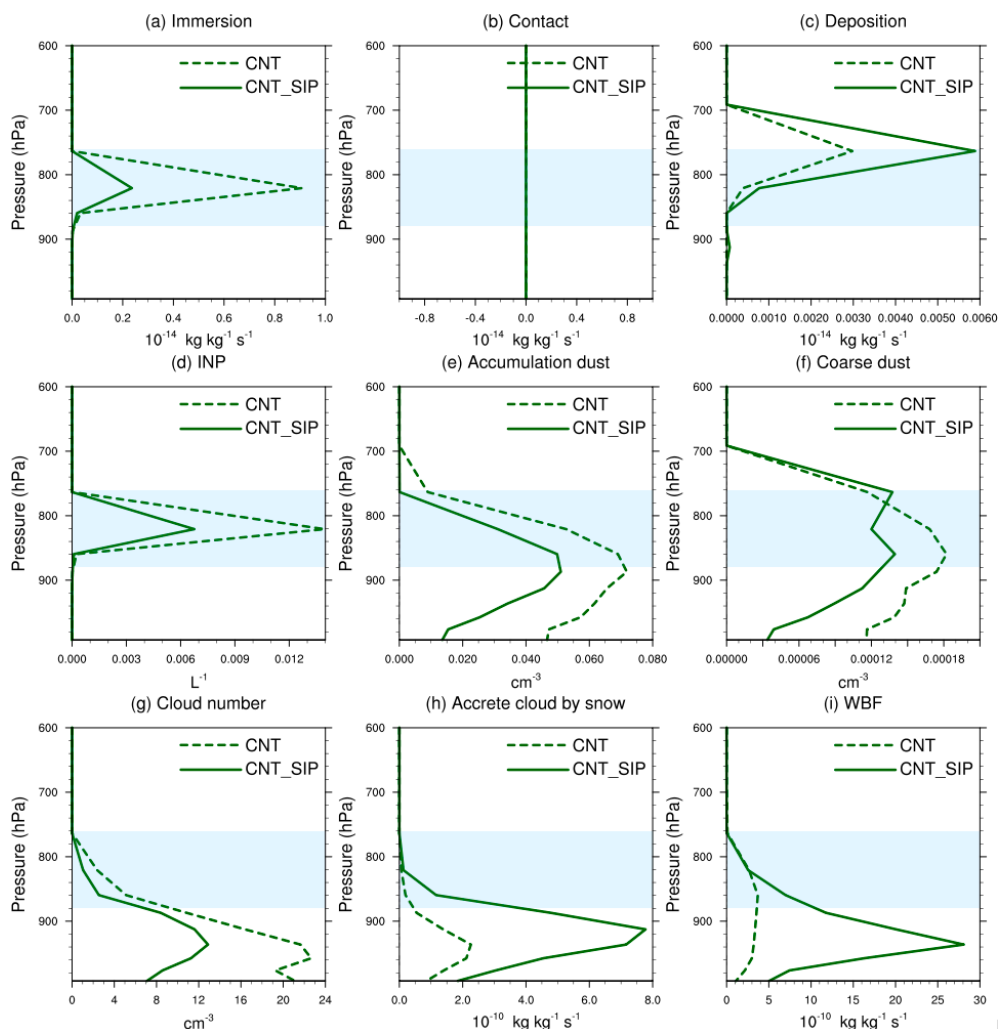
Figure 9. Vertical profiles of (a) ice production rate from immersion freezing of cloud water, (b) ice production rate from contact freezing of cloud water, (c) ice production rate from homogeneous and heterogeneous deposition nucleation, (d) immersion freezing INP number concentration, (e) cloud-borne dust number in accumulation mode, (f) cloud-borne dust number in coarse mode, (g) cloud droplet number concentration, (h) accretion rate of cloud water by snow, and (i) WBF process rate from CNT and CNT_SIP experiments averaged over the single-layer mixed-phase cloud period. Light blue shadings indicate the ice nucleation regime.
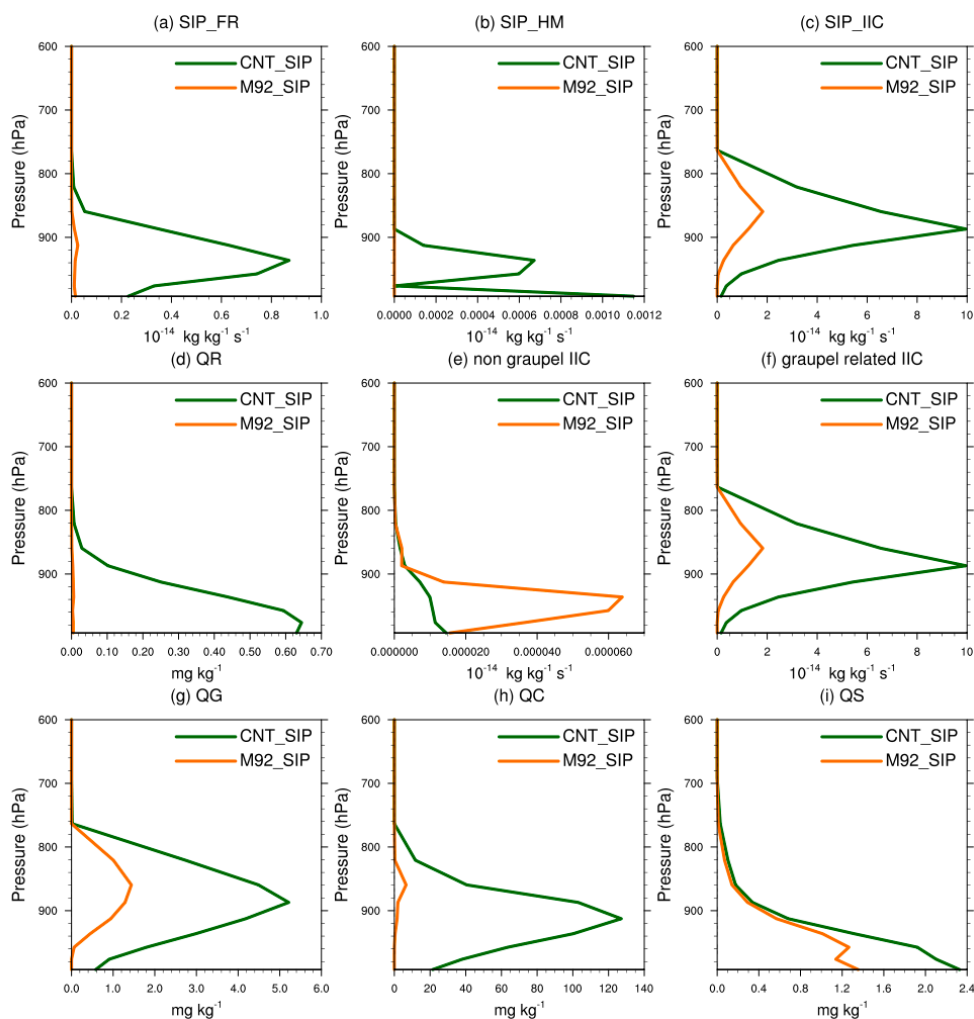
691

692   Figure 10. Vertical profiles of (a) rain droplet shattering rate during freezing (FR), (b)

693   rime splintering rate (HM), (c) ice-ice collision fragmentation rate (IIC), (d) rain water

694   mixing ratio (Qr, in unit of mg kg^{-1}), (e) non graupel related ice-ice collision

695   fragmentation rate, (f) graupel related ice-ice collision fragmentation rate, (g) graupel

696   mass mixing ratio (Qg, in unit of mg kg^{-1}), (h) cloud water mass mixing ratio (Qc, in unit

697   of mg kg^{-1}), and (i) snow mass mixing ratio (Qs, in unit of mg kg^{-1}) from the CNT_SIP

698   and M92_SIP experiments.